Analysis of semiconductor laser dynamics under gigabit rate modulation

メタデータ	言語: eng
	出版者:
	公開日: 2017-10-03
	キーワード (Ja):
	キーワード (En):
	作成者:
	メールアドレス:
	所属:
URL	http://hdl.handle.net/2297/3727

Analysis of semiconductor laser dynamics under gigabit rate modulation

Moustafa Ahmed[a)]
Department of Physics, Faculty of Science, Minia University, 61519 El-Minia, Egypt

Minoru Yamada[b)]
Division of Electrical Engineering and Computer Science, Graduate School on Natural Science and Technology, Kanazawa University, Kakuma-machi, Kanazawa 920-1192, Japan

Safwat W. Z. Mahmoud[c)]
Department of Physics, Faculty of Science, Minia University, 61519 El-Minia, Egypt

A theoretical study of the dynamics of semiconductor lasers subjected to pseudorandom digital modulation at gigabit rates is presented. The eye diagram, turn-on jitter (TOJ), and power fluctuations in the modulated laser wave form are analyzed. The study is based on numerical large-signal analysis of the laser rate equations. Influences of the biasing and modulation currents on the eye diagram and TOJ are examined. The degree of eye opening is measured in terms of a Q factor of the laser signal analogous to the Q factor determining the bit-error rate in transmission systems. Influence of optimizing both the sampling and decision times on the signal Q factor is modeled. We show that the most eye opening corresponds to shortening the sampling time associated with lengthening the decision time. We also assess the relative contributions of the laser intrinsic noise and pseudorandom bit pattern to the TOJ. The results show that the bit pattern is the major contributor to the TOJ when the setting time of the relaxation oscillation is longer than the bit slot. © *2007 American Institute of Physics*. [DOI: 10.1063/1.2434803]

I. INTRODUCTION

Semiconductor lasers are the most representative radiation sources in modern technological systems, such as optical communications and optical disk. However, the laser radiation inherently exhibits intensity noise[1] that affects the system performance. The intrinsic origins of this noise are inclusion of the spontaneous emission into the lasing mode and processes of electron-hole recombination.[2,3] Moreover, the laser exhibits inferior characteristics during the transient regime, such as time delay of the laser turn on.[4,5] The turn-on delay is defined as the time interval between the onset of the electrical pulse and the resulting optical pulse. In digital transmission systems where the laser is subjected to direct digital modulation by "on-off keying," the turn-on delay is not a fixed quantity but exhibits random fluctuations giving rise to jitter. This turn-on jitter (TOJ) is defined as the standard deviation of the random turn-on delay. The TOJ reduces the bit rate and acts as a limiting factor in the performance of transmission systems especially those working at gigabit transmission rates.[6,7] The TOJ comes from both the intrinsic intensity noise and the history of the bits preceding each 1 bit in the pseudorandom modulation pattern. The bit-pattern-induced TOJ was proven as a main cause of chirp noise,[8] which gives a bit-error rate (BER) floor.[9] Gustavsson *et al.* showed that the bit-pattern-induced TOJ is enhanced when the bit slot becomes shorter than the setting time of the relaxation oscillations.[10] Although several experimental and theoretical studies have analyzed the TOJ,[11–20] inadequate

attention has been paid to differentiate the relative contributions of the intrinsic noise and bit pattern to the TOJ specially under non-return-to-zero (NRZ) modulation.[21] On the other hand, the laser fluctuations are likely amplified either intrinsically by mode competition phenomena[22] or extrinsically due to external optical feedback,[23] which enhances the TOJ and BER.[11,12,24] Therefore, modeling of laser fluctuations and evaluation of the TOJ are essential to understand the laser behavior and estimate its digital modulation performance.

The dynamic response of digitally modulated lasers is examined qualitatively and visually by the so-called eye diagram.[25] The eye diagram is constructed by dividing the laser wave form into segments of an equal number of bits and overlying each other. The degree of eye opening, which is an indicator of the modulation performance, is degraded by the existence of the intrinsic noise and TOJ.[7] It is of practical interest to determine the time interval within which the eye diagram is most open, which is traditionally measured as the maximum on-off ratio of the signal power.[25] In digital transmission systems and for such a purpose, the detected signal is sampled by the decision circuit over a period called "sampling time" T_s within the bit slot T_b. The sampling is decided at an instant called "decision time" T_d which is determined through clock recovery. The relations of T_s and T_d with T_b are $0 < T_s \leq T_b$ and $0 \leq T_d \leq T_b - T_s$ as illustrated in the scheme of Fig. 1 of a 3-bit-long eye diagram. The best sampling and decision times correspond to the situation in which the power on-off ratio is maximized. The choice of the power on-off ratio as a measure of the eye opening, however, becomes awkward when the amplitude of the associated power fluctuations in either signal level is large and may

---

[a)]FAX: 20-86-2363011; Electronic mail: moustafaahmed@yahoo.com
[b)]FAX: 81-76-234-4870; Electronic mail: myamada@t.kanazawa-u.ac.jp
[c)]FAX: 20-86-2363011; Electronic mail: safwatwilliam@yahoo.com
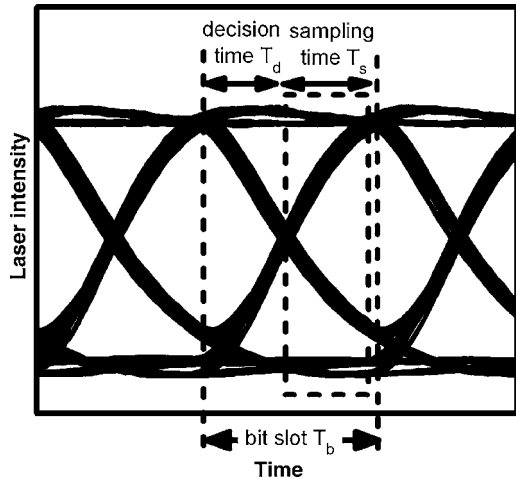
FIG. 1. Illustrative figure of a 3-bit-long eye diagram indicating the sampling and decision times.

generate errors in estimating the modulation performance. Nevertheless, theoretical modeling of the optimum choice of the sampling and decision times is still lacking.

Balle et al.[8] introduced statistical analysis of the spectral properties of laser pulses emitted under both return-to-zero (RZ) and NRZ modulation schemes with gigabit rates and investigated the TOJ and chirp noise. They showed that the bit-pattern-induced TOJ is minimum when the laser is biased slightly under threshold.[8] However, such analysis was limited to injection currents near (under and above) threshold while fixing the modulation current at a higher value. Balle et al.[8] also examined the dependence of the BER of the laser emission on the sampling time but at a fixed decision time demonstrating that the BER drops to lower values with the increase of the sampling time.

In this paper, we introduce comprehensive numerical simulations of the modulation characteristics of semiconductor lasers subjected to digital NRZ modulation with gigabit rates. The modulation performance of the laser is determined in terms of the TOJ and the quality of the eye diagram. The degree of eye opening is evaluated in terms of a laser signal Q factor Q_{signal}, which defines the difference between the average intensities in the 1 and 0 states relative to summation of the corresponding standard deviations. This factor is analogous to the Q factor that determines the BER in transmission systems.[25] We introduce numerical modeling of the optimum choice of the sampling and decision times for maximizing the Q_{signal} and compare the results with those investigated by Balle et al.[8] Dependences of the modulation characteristics on both the biasing and modulation currents as well as the bit rate are presented. We also assess the relative contributions of the laser intrinsic noise and pseudorandom bit pattern to the TOJ. The results show that when the setting time of the relaxation oscillations is longer than the bit slot, the eye diagram exhibits splitting of the turn-on edge associated with enhanced TOJ. Our results on the TOJ agree with the experimental observation of Shen[17] that the laser exhibits strong TOJ when biased under threshold. When the laser is biased well above threshold, we show that the intrinsic noise entirely dominates the contribution to the TOJ un-

der low-speed modulation. Under high-speed modulation, the pattern effect becomes the major contributor as long as the setting time of the relaxation oscillation is longer than the bit slot.

In the following section, we present the theoretical model of semiconductor laser characteristics under digital modulation. In Sec. III, numerical procedures of simulating the eye diagram and evaluation of TOJ are given. The results of dependency of the eye diagram, TOJ, and signal Q factor on the biasing and modulation currents and the bit rate are also given in Sec. III. The work is concluded in Sec. IV.

II. THEORETICAL MODEL

In this section, we introduce the theoretical framework of simulating the digital modulation characteristics of semiconductor lasers. The dynamics of semiconductor lasers under direct digital modulation are simulated by numerical large-signal analysis of the rate equations of the photon number $S(t)$ and injected electron number $N(t)$:

$$\frac{dS}{dt} = (G - G_{\text{th}})S + \frac{a\xi}{V}N + F_S(t), \tag{1}$$

$$\frac{dN}{dt} = \frac{1}{e}I(t) - AS - \frac{N}{\tau_s} + F_N(t), \tag{2}$$

where G is the optical gain (per second) which is described by the nonlinear form[26]

$$G = A - BS, \tag{3}$$

where A and B are the linear and nonlinear (suppressed) gain coefficients. They are given by

$$A = \frac{a\xi}{V}(N - N_g), \tag{4}$$

$$B = \frac{9}{2}\frac{\pi c}{\varepsilon_0 n_r^2 \hbar \lambda_0}\left(\frac{\xi\tau_{\text{in}}}{V}\right)^2 a|R_{cv}|^2(N - N_s). \tag{5}$$

In the above equations, a is a tangential gain coefficient, ξ is the confinement factor of the electric field to the active region whose volume is V and refractive index is n_r, λ_0 is the emission wavelength, $\hbar$ is the reduced Planck constant, c and ε_0 are the speed of light and permittivity in vacuum, N_g is the electron number at transparency, τ_{in} is the electron intraband relaxation time, N_s is an electron number characterizing the nonlinear gain, R_{cv} is the dipole moment, e is the electron charge, and τ_s is the electron lifetime due to spontaneous emission. G_{th} represents the threshold gain level. The term BS measures the gain suppression which affects the damping rate of the relaxation oscillation.[27]

The direct digital modulation is included in the current term $I(t)$, which represents the stream of coded bits of the modulating electrical signal:

$$I(t) = I_b + I_m f_m(t), \tag{6}$$

where I_b is the direct biasing current of the laser and I_m is the modulation current which decides the modulation depth of the laser. $f_m(t)$ is a time varying function with either 0 or 1 level describing the bit format of the modulating current; it

commonly describes either a NRZ or a RZ pseudorandom bit generation.

In Eqs. (1) and (2), the terms $F_S(t)$ and $F_N(t)$ are Langevin noise sources describing the intrinsic fluctuations in $S(t)$ and $N(t)$ that are associated with quantum transitions of electrons between the valence and conduction bands. These noise sources have Gaussian statistics and are δ correlated satisfying the following correlations:[3]

$$\langle F_S(t)F_S(t')\rangle = V_{SS}\delta(t - t'), \tag{7}$$

$$\langle F_N(t)F_N(t')\rangle = V_{NN}\delta(t - t'), \tag{8}$$

$$\langle F_S(t)F_N(t')\rangle = V_{SN}\delta(t - t'), \tag{9}$$

where δ is the Dirac delta function. The autocorrelation variances V_{SS} and V_{NN} and the cross-correlation variance V_{SN} define the moments of the noise sources $F_S(t)$ and $F_N(t)$. These variances are determined from the rate equations as will be given in the next section.

The power $P(t)$ emitted from the front facet of the laser cavity is calculated from the fluctuating photon number $S(t)$ via the relationship

$$P(t) = \frac{h\nu c}{2n_r L} \frac{(1 - R_f)\ln(1/R_f R_b)}{(1 - \sqrt{R_f R_b})(1 - \sqrt{R_f/R_b})} S(t), \tag{10}$$

where n_r and L are the refractive index and length of the active region, respectively, $h\nu$ the photon energy of the emitted light, and R_f and R_b the power reflectivities of the front and back facets, respectively.

III. NUMERICAL SIMULATION AND RESULTS

The rate equations (1) and (2) are solved numerically by means of the fourth-order Runge-Kutta method assuming square pulses of the modulating current in Eq. (6). The time step of integration Δt is set to be as short as 2 ps, which corresponds to a cut-off Fourier frequency $(=1/\Delta t)$ of the laser wave form that is much higher than the relaxation frequency f_r. This very small value of Δt helps to treat the δ functions numerically in Eqs. (7)–(9) and to generate the noise sources $F_S(t_i)$ and $F_N(t_i)$ at each instant t_i as[3]

$$F_S(t_i) = \sqrt{\frac{V_{SS}(t_i)}{\Delta t}} g_S, \tag{11}$$

$$F_N(t_i) = \sqrt{\frac{V_{NN}(t_i) + V_{NS}^2(t_i)/V_{SS}(t_i)}{\Delta t}} g_N - \frac{V_{NS}(t_i)}{V_{SS}(t_i)} F_S(t_i), \tag{12}$$

where g_S and g_N are independent Gaussian random numbers with means of zero and variances of unity. The variances $V_{SS}(t_i)$, $V_{NN}(t_i)$, and $V_{SN}(t_i)$ are evaluated from the photon number $S(t_{i-1})$ and electron number $N(t_{i-1})$ at the preceding time t_{i-1} supposing a quasi-steady-state $(dS/dt \approx dN/dt = 0)$ over Δt. They are given by[3]

$$V_{SS}(t_i) = 2\frac{a\xi}{V}[S(t_{i-1}) + 1]N(t_{i-1}), \tag{13}$$

TABLE I. Typical values of the parameters of a single-mode InGaAsP laser emitting with $\lambda = 1.55$ μm.

Symbol	Meaning	Value	Unit
a	Tangential gain coefficient	7.85×10^{-12}	s^{-1}
ξ	Field confinement factor	0.2	$\cdots$
V	Volume of the active region	60	μm^3
L	Length of the active region	250	μm
n_r	Refractive index of the active region	3.56	$\cdots$
Ng	Electron number at transparency	5.31×10^7	$\cdots$
τ_{in}	Electron intraband relaxation time	0.13	ps
$\lvert R_{c\nu}\rvert^2$	Squared absolute value of the dipole moment	9.53×10^{-57}	C^2 m^2
Ns	Electron number characterizing nonlinear gain	4.05×10^7	$\cdots$
B_{eff}	Effective rate of nonradiative recombination	3.9×10^{-16}	s^{-1}
G_{th}	Threshold gain level	8.84×10^{10}	s^{-1}

$$V_{NN}(t_i) = 2\left[\frac{1}{\tau_s} + \frac{a\xi}{V}S(t_{i-1})\right]N(t_{i-1}), \tag{14}$$

$$V_{NS}(t_i) = -\frac{a\xi}{V}N(t_{i-1})[S(t_{i-1}) + 1] + N_g S(t_{i-1}). \tag{15}$$

The laser is modulated with a NRZ pseudorandom bit stream (PRBS) of length $2^7 - 1$. We consider four bit slots $T_b = 100$, 125, 200, and 400 ps, which correspond to high gigabit rates $B = 1/T_b = 10$, 8, 5, and 2.5 Gbits/s, respectively. The integration is performed over multiple lengths of PRBSs in order to collect significant statistics of modulation parameters. The modulation characteristics are simulated as functions of both the biasing current I_b and modulation depth I_m. A Fabry-Pérot InGaAsP laser emitting with $\lambda = 1.55$ μm is considered in the simulation. The nonradiative recombination processes are taken into account in the rate equation through the lifetime τ_s as

$$\frac{1}{\tau_s} = B_{eff}N/V, \tag{16}$$

where B_{eff} is the effective rate of electron recombination including both the radiative and nonradiative recombination processes. Typical parametric values of the considered laser are given in Table I. The corresponding threshold current is $I_{th} = 3.3$ mA.

A. Eye diagram

In the present simulations, the eye diagram is constructed by dividing the stream of $P(t)$ into 3-bit-long sequences and overlying each other. Figures 2(a) and 2(b) show two examples of the eye diagram at bit rates of $B = 2.5$ and 10 Gbits/s, respectively. The biasing current is $I_b = 2I_{th}$, i.e., the laser is biased well above threshold, and the modulation current is $I_m = 4I_{th}$. Both eye diagrams show the relaxation oscillations that characterize the transient regime of the laser. In this case of above-threshold biasing, the oscillations are characterized by high damping rate as predicted by the small-signal analysis.[27,28] The relaxation oscillation is
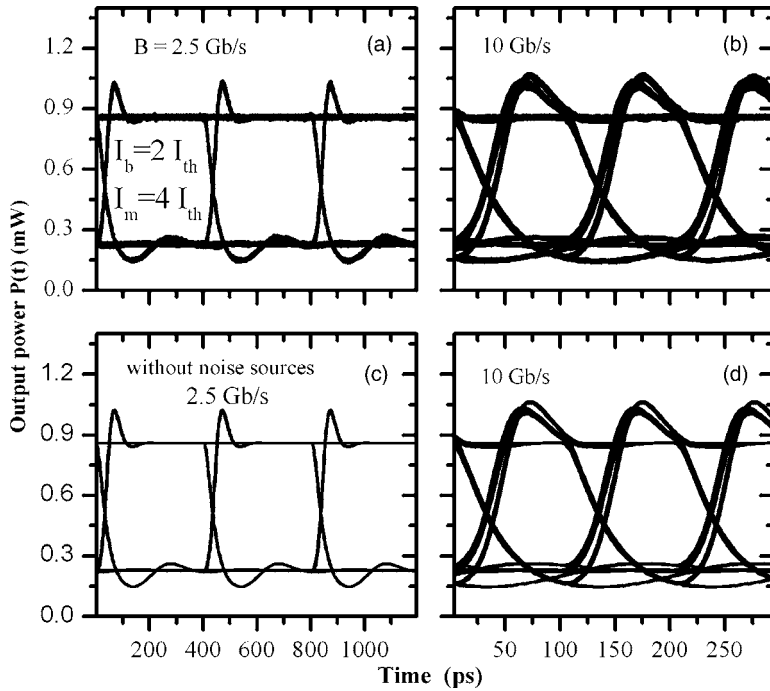
FIG. 2. Example of the simulated eye diagrams for (a) $B=2.5$ Gbits/s, and (b) $B=10$ Gbits/s, when $I_b=2I_{th}$ and $I_m=4I_{th}$. (c) and (d) plot the corresponding eye diagrams when ignoring the noise sources. The eye is well open at $B=2.5$ Gbits/s, while the turn-on time delay partially closes the eye at $B=10$ Gbits/s. Ignoring the noise sources results in thinner borders of the eye diagram.

associated with the inferior property of turn-on time delay which induces errors in identifying the logic state of the bit. This effect is significant when $B=10$ Gbits/s compared with the case of $B=2.5$ Gbits/s; TOJ is 4.73 ps for the former and 2.58 ps for the latter. The strong TOJ characterizing the higher bit rate is a manifest of the pseudorandom bit pattern (history of 0 bit preceding each 1 bit). This effect arises when the biasing current I_b corresponds to a setting time of the relaxation oscillation ($t_r=1/f_r$) longer than the bit slot T_b. Following the small-signal analysis,[28] it can be shown that t_r is inversely proportional to the biasing level I_b,

$$t_r = \frac{1}{f_r} \approx 2\pi \left/ \sqrt{\frac{a\xi}{V}\left(1 + \frac{B}{G_{th}}\frac{I_b - I_{th}}{e}\right)\frac{I_b - I_{th}}{e}}\right. . \quad (17)$$

This relation is plotted in Fig. 3 which indicates that t_r is approximately equal to the bit slots $T_b=100$, 125, 200, and 400 ps when $I_b \approx 4.3I_{th}$, $3.2I_{th}$, $2.2I_{th}$, and $1.3I_{th}$, respectively. The figure shows that t_r decreases rapidly near $I_b=I_{th}$, which predicts rapid drop of the TOJ with the increase of I_b for longer bit slot T_b (or lower B). In the region of high I_b, t_r
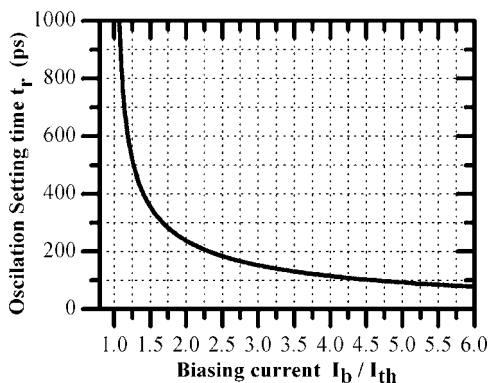
becomes less sensitive to the variation of I_b which indicates stronger TOJ under high B. This result interprets the reason why the TOJ limits the modulation performance at high bit rates.

In Fig. 2(a) since $t_r=240$ ps is short enough compared with T_b, the eye is well open with the 1 and 0 states of the output power being well defined. The intrinsic intensity noise is the main contributor to the TOJ as well as the fluctuations seen on the eye borders. To confirm this effect, we plot in Figs. 2(c) and 2(d) the corresponding eye diagrams simulated by dropping the Langevin noise sources from rate equations (1) and (2). Figure 2(c) shows much thinner borders of the eye. The eye diagram in Fig. 2(b) of $B=10$ Gbits/s is partially closed and characterized by a budge on the top. The high TOJ appears as splitting of both the turn-on transition and the budge on the eye top into two different paths. Figure 2(d) shows that ignoring the noise sources suppresses the power fluctuations, making the eye borders thinner. However, the dual split of the turn-on edge is still seen as the TOJ decreases a little to 4.41 ps confirming its origin from the bit pattern. Nevertheless, the influence of intrinsic laser noise is found to develop with lowering I_b and/or I_m which corresponds to degradation of the degree of laser coherency.

B. Variations of eye diagram with biasing and modulation currents

Under digital modulation, both magnitudes of the biasing current I_b and modulation current I_m influence the laser output and modulation characteristics.[10,17] Here, we examine how the choices of both I_b and I_m affect the eye diagram characteristics. Figures 4 and 5 plot the eye diagrams simulated at I_b and I_m lower and higher than those in Fig. 2. Figure 4 illustrates the effect of changing I_b while keeping I_m at $4I_{th}$. Figures 4(a)–4(c) correspond to $B=2.5$ Gbits/s, Figs. 4(d)–4(f) to 5 Gbits/s, and Figs. 4(g)–4(i) to 10 Gbits/s when $I_b=0.8$, 1.5, and $3I_{th}$, respectively. When the laser is

FIG. 3. Plot of the setting time t_r of the relaxation oscillation versus the biasing current I_b. Near threshold, t_r decreases rapidly with the increase of I_b, while the decrease becomes very slow in the high-biasing region.
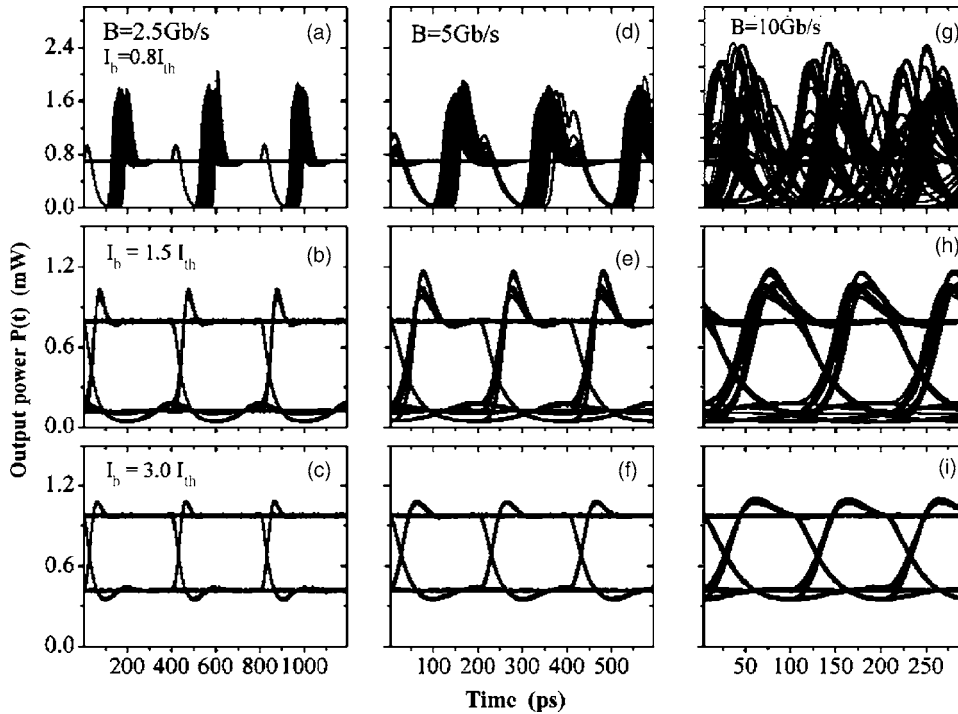
FIG. 4. Eye diagrams at modulation depth $I_m = 4I_{th}$ and different biasing currents $I_b = 0.8$, 1.5, and $3.0I_{th}$ for three bit rates of $B = 2.5$, 5, and 10 Gbits/s. The eye quality improves by increasing I_b, where both the TOJ and thickness of the eye borders decrease.

biased under threshold, $I_b = 0.8I_{th}$, Figs. 4(a), 4(d), and 4(g) show that the laser exhibits very strong TOJs of 19, 15.5, and 32.2 ps, respectively, as well as enhanced relaxation oscillation in the 1 level. The effect of strong TOJ is most pronounced in the case of the highest bit rate, $B = 10$ Gbits/s, which results in a completely closed eye. The eye is partially open when $B = 5$ Gbits/s and is most improved when $B = 2.5$ Gbits/s. By increasing I_b to $1.5I_{th}$, t_r becomes comparable to T_b for $B = 2.5$ Gbits/s resulting in a weak TOJ and a well-open eye diagram as shown in Fig. 4(b). When $B = 5$ and 10 Gbits/s, Figs. 4(e) and 4(h) indicate less significant TOJs of 6.2 and 6.4 ps, respectively, with the eye diagram of

$B = 5$ Gbits/s being more defined. However, the transients are split into three paths because $t_r \approx 360$ ps is still longer than T_b. By further increase of I_b to $3I_{th}$, the eye diagram is most defined when $B = 2.5$ Gbits/s as shown in Fig. 4(c). In Figs. 4(f) and 4(i), the TOJ is more suppressed to 1.9 ps when $B = 5$ Gbits/s and 2.68 ps when $B = 10$ Gbits. While less significant split of the turn-on transition is still seen in Fig. 4(i), it disappears in Fig. 4(f) because $t_r \approx 150$ ps is shorter than T_b. These results necessitate the increase of I_b in order to improve the eye diagram quality and laser performance under high-speed modulation.

Figure 5 illustrates the influence of varying the modula-
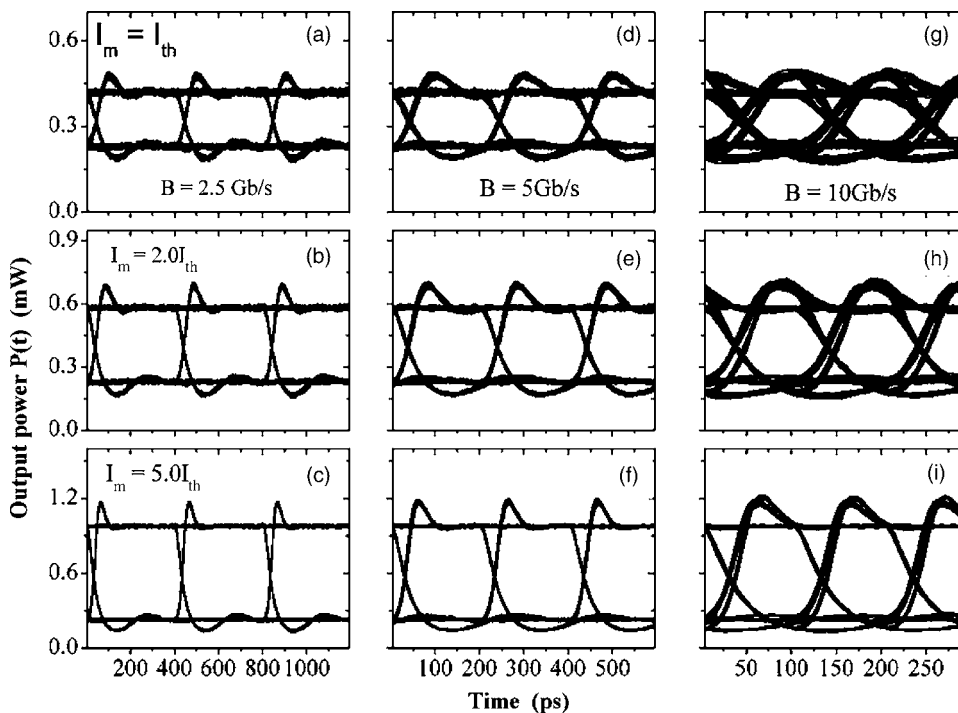
FIG. 5. Eye diagrams at a fixed biasing current $I_b = 2I_{th}$ and different modulation depths $I_m = I_{th}$, $2I_{th}$, and $5I_{th}$ for $B = 2.5$, 5, and 10 Gbits/s. The eye quality improves by increasing I_m.

tion depth I_m on the eye diagram while keeping the biasing current above threshold, $I_b=2I_{th}$. Figures 5(a)–5(c) correspond to B=2.5 Gbits/s, Figures 5(d)–5(f) to 5 Gbits/s, and Figs. 5(g)–5(i) to 10 Gbits/s when $I_m=I_{th}$, $2I_{th}$, and $5I_{th}$, respectively. In these cases, $t_r \approx 240$ ps, which is shorter than T_b of B=2.5 Gbits/s, comparable to T_b of B=5 Gbits/s, but longer than T_b of B=10 Gbits/s. Therefore, the split of the turn-on edge disappears in Figs. 5(a)–5(c) of B =2.5 Gbits/s but is apparent in Figs. 5(g)–5(i) of B =10 Gbits/s. When B=2.5 Gbits/s, increasing I_m results in an increase of the power $P_1(t)$ in the 1 level accompanied with reduction of power fluctuations. The TOJ also reduces from 3.59 ps in Fig. 5(a) to 3.0 ps in Fig. 5(b) and to 2.5 ps in Fig. 5(c). This reduction contributes to improvement of the eye diagram. Similarly, the characteristics of the eye diagrams of Figs. 5(d)–5(f) improve with the increase of I_m, but the eye borders are thicker than those of Figs. 5(a)–5(c). For the highest bit rate B=10 Gbits/s, the TOJ is stronger and the turn-on edge is split into two paths. In Fig. 5(g), the splitting is shown also in the bulge on top and the eye is degraded. Increasing I_m results in an increase of the eye opening as shown in Figs. 5(h) and 5(i) where the eye edges and upper levels become more defined. These results point to improvement of the eye quality by increasing I_m.

It should be noted that the above simulated eye diagrams describe the intrinsic digital modulation characteristics of the laser rather than of an entire laser-based transmission system. In such a system, dominating thermal receiver noise is superimposed on the detected signal which results in less distinct eye diagrams. The above investigated dependencies of the eye diagram on I_b and I_m are in good qualitative agreement with those simulated and recorded by Gustavsson *et al.*[10] and Valle and Pesquera[20] on VCSELs.

C. Dependences of TOJ on biasing and modulation currents

As given in the above discussion, the TOJ is an important indicator of the quality of the eye diagram especially under higher bit rate. Therefore, it is essential to examine influences of both the biasing and modulation currents and bit rate on the TOJ in order to gain insight on how to control the laser diode and its modulation performance. We define the turn-on delay as the time at which the power $P_1(t)$ in the 1 bit first surpasses 50% of the summation of the steady state powers corresponding to I_b and I_m, i.e., $P_1(t)$ crosses the middle of the eye diagram. Figure 6(a) plots dependency of the TOJ on I_b for B=2.5, 5, 8, and 10 Gbits/s. The calculations are done at $I_m=4I_{th}$. The figure shows that when the laser is biased under threshold, $I_b<I_{th}$, the TOJ maintains high and almost constant values until $I_b \approx 0.5I_{th}$, and then decreases rapidly with the increase of I_b. Near the free-biasing limit, $I_b=0$, where the intrinsic noise is pronounced, the TOJ is highest when B=2.5 Gbits/s and lies within a lower narrow range for higher bit rates. This result means that near $I_b=0$, the contribution of intrinsic noise to the TOJ is more enhanced with the decrease of B. Above the threshold current and depending on the magnitude of I_b, the decrease of the TOJ with the increase of I_b becomes slower.
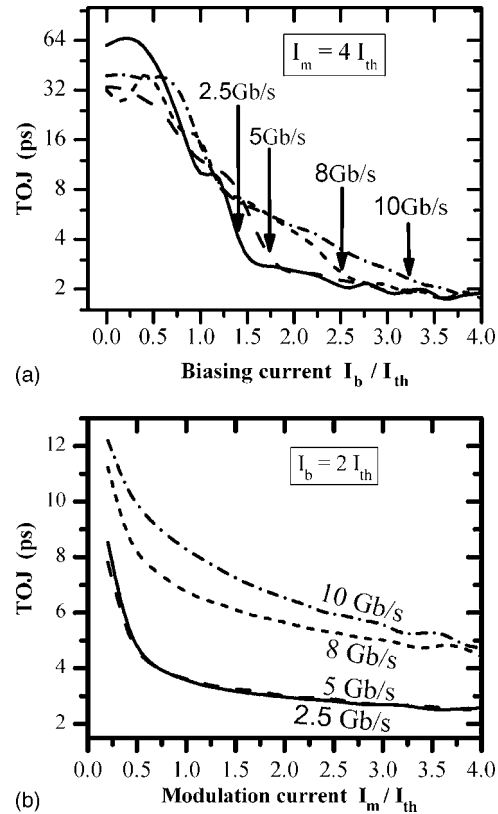
FIG. 6. Dependencies of TOJ on (a) I_b with $I_m=4I_{th}$ and (b) I_m with I_b =$2I_{th}$ for B=2.5, 5, 8, and 10 Gbits/s. For a given B, the TOJ generally decreases with the decrease of either I_b or I_m. Above threshold, the TOJ increases with the increase of B.

The calculated values of the TOJ around $I_b=I_{th}$ are comparable to those calculated by Balle *et al.*[8] In the high-biasing region, $I_b>3.2I_{th}$, the TOJ saturates at about 2 ps regardless of the value of B. The magnitude of I_b at which the turning to this slower rate happens increases with the increase of B; for example, it is $I_b \approx 1.4I_{th}$ when B=2.5 Gbits/s, $I_b \approx 1.7I_{th}$ when B=5 Gbits/s, $I_b \approx 2.5I_{th}$ when B=8 Gbits/s, and $I_b \approx 3.2I_{th}$ when B=10 Gbits/s. Since these turning currents are comparable to those deduced from Eq. (17) for the corresponding bit slots, it can be understood that the strong TOJ is a pattern effect because $T_b<t_r$. This pattern effect can then be diminished by raising I_b when the bit rate B is increased. A similar behavior of the TOJ with $I_b>I_{th}$ is observed in experiment by Weber *et al.*[18]

Figure 6(b) plots dependency of the TOJ on I_m at a fixed biasing current above threshold of $I_b=2I_{th}$. The figure shows that at a given bit rate B, the TOJ decreases rapidly from about 12 ps with the increase of I_m in the region of $I_m \lesssim I_{th}$. The TOJ then decreases slowly with further increase of I_m. This means that the TOJ depends not only on I_b but also on I_m, which is consistent with the predictions and measurements of Shen,[17] and Valle and Pesquera.[20] The figure shows also that at a fixed value of I_m, especially when $I_m>0.5I_{th}$, the increase of B beyond 5 Gbits/s results in an increase of the TOJ, whereas decreasing B to 2.5 Gbits/s has almost no change. This effect is also due to the bit-pattern effect that develops with the increase of B. The calculated values of the TOJ almost agree with those measured in experiments.[17,18]

D. Laser signal Q factor

Of practical interest is to determine the most open section of the eye diagram over which statistics on laser power fluctuations are frequently taken.[6] In this paper, we determine the opening of the eye diagram in terms of a characteristic quantity analogous to the Q factor that controls the BER in transmission systems.[25] We call this factor "laser signal Q factor" Q_{signal}, and define it as

$$Q_{signal} = \frac{\bar{P}_1 - \bar{P}_0}{\sigma_0 + \sigma_1}, \qquad (18)$$

where $\bar{P}_j$ and σ_j, with $j=0$ or 1, are the time average of the power and the standard deviation of the corresponding fluctuations in either signal level, respectively. The merit of using this factor is twofold. First, its numerator determines the difference of the power levels in the 1 and 0 levels while the denominator gives the sum of the power fluctuations. Therefore, it contains combined information on the vertical width of the eye diagram and the fluctuations around the average power of either logical level. Second it may be used as indicator to the contribution of laser noise to the BER in practical transmission systems.

The illustrative eye diagram of Fig. 1 is used to determine the most open section of the eye diagram in terms of Q_{signal} as follows. During each bit of duration T_b, the fluctuating power is sampled over different sampling times T_s with $0 < T_s \leq T_b$ and at different decision times in the range $0 < T_d \leq T_b - T_s$. For each pair of T_s and T_d, the average powers $\bar{P}_1$ and $\bar{P}_0$ and the corresponding variances σ_1^2 and σ_0^2 in the 1 and 0 levels, respectively, are calculated. These values are then used to calculate Q_{signal} via Eq. (18). The most open portion of the eye diagram then corresponds to the pair of times T_s and T_d that results in the maximum value of Q_{signal}.

In Figs. 7(a)–7(c), we show variation of Q_{signal} with T_d at different times T_s for three bit rates $B=2.5$, 5, and 10 Gbits/s, respectively, when $I_b=I_m=2I_{th}$. The figures correspond to the eye diagrams of Figs. 5(b), 5(e), and 5(h), respectively. The figures show a common feature that the Q_{signal} is maximum when $T_s=0.2T_b$ and $T_d=0.8T_b$. This shortest sampling time and far decision point (near the end of the bit) correspond to the middle of the eye, which is the most open region as can be seen in the corresponding eye diagrams. On the other hand, the figures show another common and interesting feature that at a given decision time T_d, Q_{signal} improves with lengthening the sampling time T_s. This result agrees with the prediction of Balle *et al.*[8] that minimum BER is achieved when T_s is longest under NRZ modulation. This technique of determining the most eye opening section can be applied to determine the optimum choice of T_s and T_d that corresponds to minimum BER in transmission systems.

E. Dependences of Q_{signal} on biasing and modulation currents

Here we discuss quantitatively influences of both I_b and I_m on the eye diagram opening in terms of Q_{signal}. Figures 8(a) and 8(b) plot variations of Q_{signal} with I_b when $I_m=4I_{th}$
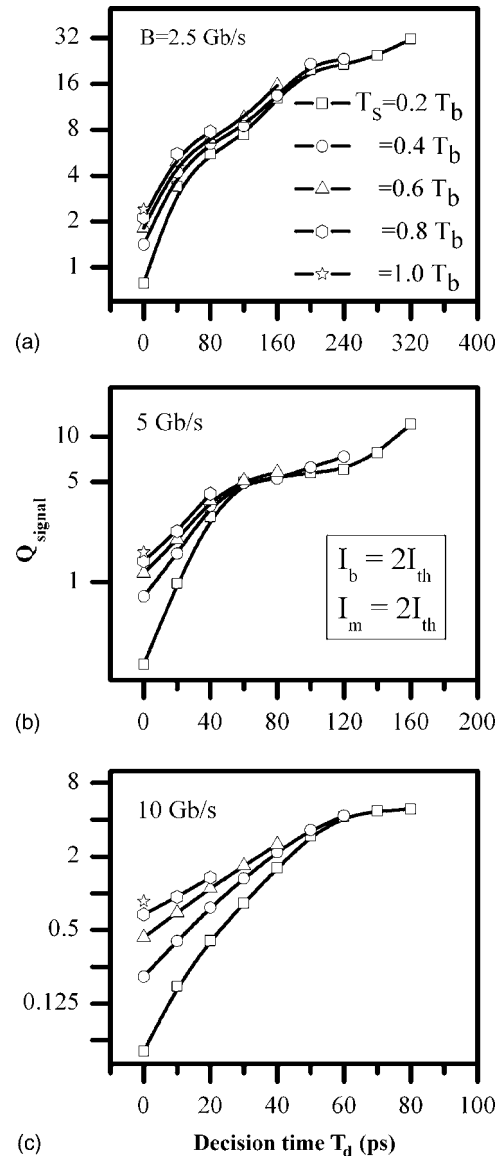
FIG. 7. Q_{signal} as a function of T_d and T_s for (a) $B=2.5$ Gbits/s, (b) $B=5$ Gbits/s, and (c) $B=10$ Gbits/s when $I_b=2I_{th}$ and $I_m=2I_{th}$. Shorter T_s with longer T_d is optimum to achieve maximum Q_{signal}.

and with I_m when $I_b=2I_{th}$, respectively, for bit rates $B=2.5$, 5, 8, and 10 Gbits/s. Figure 8(a) shows that over the entire range of I_b, Q_{signal} decreases with the increase of B, which is due to enhancement of the power fluctuations induced by the bit pattern. This effect corresponds to closure of the eye diagram and deterioration of the laser modulation performance. The entire range of Q_{signal} in this graph is 0.5–150. It is shown also that for $B=2.5$ and 5 Gbits/s, Q_{signal} increases with the increase of I_b in the under threshold region, $I_b < I_{th}$, reaching a maximum value around I_{th}. With further increase of I_b, Q_{signal} decreases over a narrow range of I_b, and finally increases. The maximum Q_{signal} is about 150 occurring at $I_b \approx I_{th}$ for $B=2.5$ Gbits/s and is about 19 occurring at $I_b=1.2I_{th}$ for $B=5$ Gbits/s. The peak shown in the cases of $B=2.5$ and 5 Gbits/s can be understood as follows. When $I_b < I_{th}$, the increase of I_b results in increase of both average powers $\bar{P}_1$ and $\bar{P}_0$ in the 1 and 0 levels, respectively. However, the increase of $\bar{P}_1$ (above threshold) is greater than that
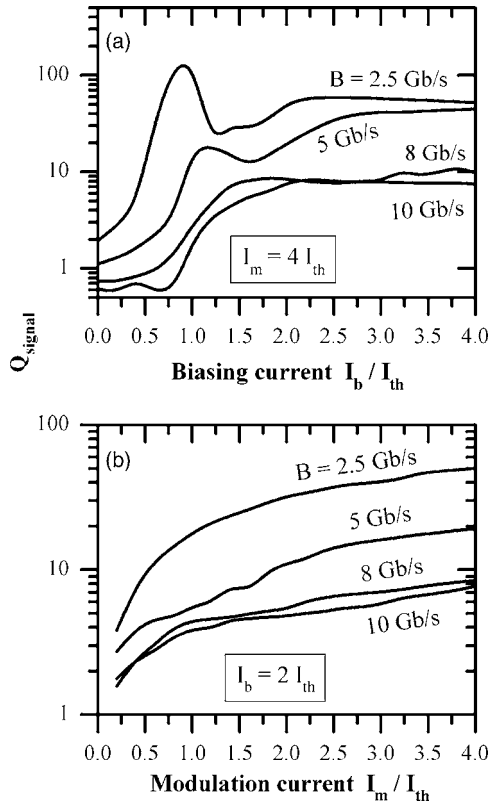
FIG. 8. Variation of Q_{signal} with (a) I_b with $I_m=4I_{th}$ and (b) I_n with $I_b=2I_{th}$ for $B=2.5$, 5, 8, and 10 Gbits/s. Q_{signal} increases with the increase of I_b and/or I_m but decreases with the increase of B.

of $\bar{P}_0$ (under threshold), which then enlarges the numerator $(\bar{P}_1-\bar{P}_0)$ of Eq. (18). The power fluctuations in the 1 level are simultaneously suppressed due to improvement of laser coherency,[3] while those in the 0 level slightly change which then decreases the denominator $(\sigma_1+\sigma_0)$. The net result is an increase of Q_{signal} with the increase of I_b as shown in the figure. On the other hand when I_b is higher than but near I_{th}, the power $P_0(t)$ exhibits relaxation oscillations with enhanced fluctuations,[3] increasing the denominator $(\sigma_1+\sigma_0)$. The powers $\bar{P}_0$ and $\bar{P}_1$ should increase with the same amount above threshold, however, the enhanced relaxation oscillations of $P_0(t)$ may increase average power $\bar{P}_0$ within the optimized sampled period T_s. Therefore, the numerator of Eq. (18) is reduced decreasing Q_{signal} and revealing the peaks shown in the figure. For $B=8$ and 10 Gbits/s, Q_{signal} is almost constant for $I_b<0.7I_{th}$, and then increases with the increase of I_b. Such increase of Q_{signal} becomes much slower when $I_b \approx 1.5I_{th}$ for $B=8$ Gbits/s and $I_b \approx 2I_{th}$ for $B=10$ Gbits/s. Figure 8(b) shows also that for a given modulation current I_m, Q_{signal} decreases as B increases with the difference of Q_{signal} getting smaller. It is also shown that for a given bit rate B, Q_{signal} increases generally in a monotonic fashion with the increase of I_m, which is due to the coupled effect of increasing the average power $\bar{P}_1$ and suppression of the power fluctuations. The entire range of Q_{signal} is 1.7–50, which is lower than the values shown in Fig. 8(a). This is because I_b is kept constant in these calculations. The obtained results indicate improvement of laser eye diagram quality with the increase of I_m and decrease of B.
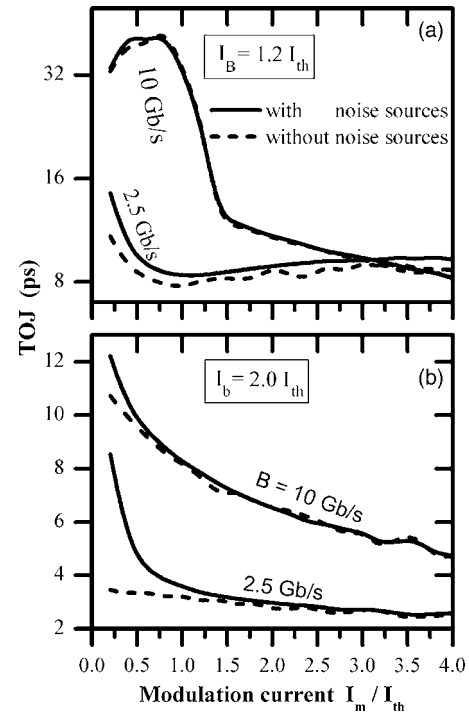
FIG. 9. Influence of ignoring noise sources on the TOJ as a function of I_m when (a) $I_b=1.2I_{th}$ and (b) $I_b=2I_{th}$. When $I_b=1.2I_{th}$, the TOJ is less affected by ignoring noise sources. When $I_b=2I_{th}$, dropping the noise sources decreases the TOJ to lower values in the low regime of I_m specially for $B=2.5$ Gbits/s.

F. Contributions of intrinsic noise and pseudorandom bit pattern to TOJ

In this section, we assess contributions of both the intrinsic noise and pseudorandom bit pattern to the TOJ. We perform this analysis numerically by comparing the TOJ calculated by both including and ignoring the Langevin noise sources in rate equations (1) and (2). Such a comparison is illustrated in Fig. 9 for bit rates $B=2.5$ and 10 Gbits/s as a function of I_m. Figure 9(a) corresponds to near-threshold biasing, $I_b=1.2I_{th}$, whereas Fig. 9(b) corresponds to far above threshold, $I_b=2I_{th}$. Figure 9(a) shows that dropping the noise sources causes almost no change in the TOJ values when $B=10$ Gbits/s and a little decrease when $B=2.5$ Gbits/s. That is, the bit-pattern effect is the main contributor to the TOJ around the threshold biasing current. This behavior agrees with the experimental measurements of Shen.[17] On the other hand, when $I_b=2I_{th}$ Fig. 9(b) shows that dropping the noise sources results in drop of the TOJ to lower values in the low regime of I_m. Such drop of the TOJ reduces with the increase of I_m and almost diminishes at $I_m>1.5I_{th}$. In the case of $B=10$ Gbits/s, the drop of the TOJ is much smaller and diminishes around $I_m=I_{th}$. This means that when biasing the laser far above threshold, the intrinsic noise becomes the major contributor to the TOJ at lower speed modulation, $B=2.5$ Gbits/s. However under high-speed modulation, $B=10$ Gbits/s, the large values of the TOJ are almost a bit-pattern effect as long as $t_r>T_b$.

IV. CONCLUSIONS

We demonstrated theoretical analysis of the dynamic characteristics of semiconductor lasers under high-speed

modulation. The study is based on a computer simulation model of the laser rate equations including a NRZ pseudorandom bit generator. Dependencies of the eye diagram and TOJ on the biasing and modulation currents as well as the bit rate were examined. We can draw the following conclusions from the obtained results.

(1) The TOJ originates from both intrinsic laser noise and the pseudorandom modulating bit pattern.

(2) Contribution of the bit pattern to the TOJ enhances when the bit slot is shorter than the setting time of the relaxation oscillation. This is seen in the eye diagram as split of the turn-on edge into distinct paths.

(3) Opening of the eye diagram is measured in terms of a Q factor of the modulated signal. The largest signal Q factor (most eye opening) corresponds to the shortest sampling time around the middle of the eye.

(4) The TOJ and eye opening improve with the increase of the biasing current and/or modulation current but degrade with the increase of the bit rate.

(5) When the laser is biased under or near threshold, the TOJ is mainly a bit-pattern effect. At far above threshold, the intrinsic noise becomes the major contributor as long as the setting time of the relaxation oscillation is shorter than the bit slot.

[1] S. Gonda and S. Mukai, IEEE J. Quantum Electron. **QE-11**, 545 (1975).

[2] G. P. Agrawal and N. K. Dutta, *Semiconductor Lasers* (Van Nostrand Reinhold, New York, 1993).

[3] M. Ahmed, M. Yamada, and M. Saito, IEEE J. Quantum Electron. **37**, 1600 (2001).

[4] K. Petermann, *Laser Diode Modulation and Noise* (Kluwer Academic, Dordrecht, 1988).

[5] P. Spano, A. Mecozzi, A. Sapia, and A. D'Ottavi, in *Third International Workshop on Nonlinear Dynamics and Quantum Phenomena in Optical Systems*, edited by R. Corbalan and R. Vilaseca (Springer-Verlag, New York, 1991).

[6] J. J. O'Rielly, J. R. F. Da Rocha, and K. Schumacher, IEE Proc.-J: Opto-electron. **132**, 309 (1985).

[7] G. P. Agrawal and T. M. Shen, Electron. Lett. **22**, 450 (1986).

[8] S. Balle, M. Homar, and M. S. Miguel, IEEE J. Quantum Electron. **31**, 1401 (1995).

[9] P. O. Andersson and K. Akermak, Electron. Lett. **28**, 471 (1992).

[10] J. S. Gustavsson, A. Haglund, J. Bengtsson, and A. Lasrsson, IEEE J. Quantum Electron. **38**, 1089 (2002).

[11] S. E. Miller, IEEE J. Quantum Electron. **22**, 16 (1986).

[12] C. R. Mirasso and E. H. Garcia, IEEE J. Quantum Electron. **30**, 2281 (1994).

[13] T. M. Shen and G. P. Agrawal, J. Lightwave Technol. **LT-5**, 653 (1987).

[14] P. Spano, A. D'Ottavi, A. Mecozzi, and S. Piazzola, Appl. Phys. Lett. **52**, 2203 (1988).

[15] E. H. Bottcher, K. Ketterer, and D. Bimberg, J. Appl. Phys. **63**, 2469 (1988).

[16] P. L. Liu and M. M. Choy, IEEE J. Quantum Electron. **25**, 1767 (1989).

[17] T. M. Shen, J. Lightwave Technol. **7**, 1394 (1989).

[18] A. G. Weber, W. Ronghan, E. H. Bottcher, M. Schell, and D. Bimberg, IEEE J. Quantum Electron. **28**, 441 (1992).

[19] C. R. Mirasso, P. Colet, and M. S. Miguel, IEEE J. Quantum Electron. **29**, 23 (1993).

[20] A. Valle and L. Pesquera, IEEE J. Quantum Electron. **42**, 435 (2006).

[21] K. Obermann, S. Kindt, and K. Petermann, IEEE Photonics Technol. Lett. **8**, 31 (1996).

[22] M. Ahmed and M. Yamada, IEEE J. Quantum Electron. **38**, 682 (2002).

[23] M. Ahmed and M. Yamada, J. Appl. Phys. **95**, 7573 (2004).

[24] G. P. Agrawal and T. M. Shen, J. Lightwave Technol. **LT-4**, 58 (1986).

[25] G. P. Agrawal, *Fiber-Optic Communication Systems* (Wiley, New York, 2002).

[26] M. Yamada and Y. Suematsu, J. Appl. Phys. **52**, 2653 (1981).

[27] S. Abdulrhmann, M. Ahmed, and M. Yamada, Opt. Rev. **9**, 260 (2002).

[28] M. Yamada and T. Higashi, IEEE J. Quantum Electron. **27**, 380 (1991).